Cold Spring Harbor Laboratory

Laura Jimenez
Lyon Lab

05/13/14

Journal Club

Quantifying Absolute Protein Synthesis Rates Reveals Principles Underlying Allocation of Cellular Resources

Gene-Wei Li,[1,2,3,*] David Burkhardt,[2,4] Carol Gross,[2,4,5] and Jonathan S. Weissman[1,2,3,*]
[1]Department of Cellular and Molecular Pharmacology, Howard Hughes Medical Institute
[2]California Institute of Quantitative Biosciences
[3]Center for RNA Systems Biology
[4]Department of Microbiology and Immunology
[5]Department of Cell and Tissue Biology
University of California, San Francisco, San Francisco, CA 94158, USA
*Correspondence: gene-wei.li@ucsf.edu (G.-W.L.), weissman@cmp.ucsf.edu (J.S.W.)
http://dx.doi.org/10.1016/j.cell.2014.02.033

Cell

Figure1

Absolute Quantification of Protein Synthesis Rates

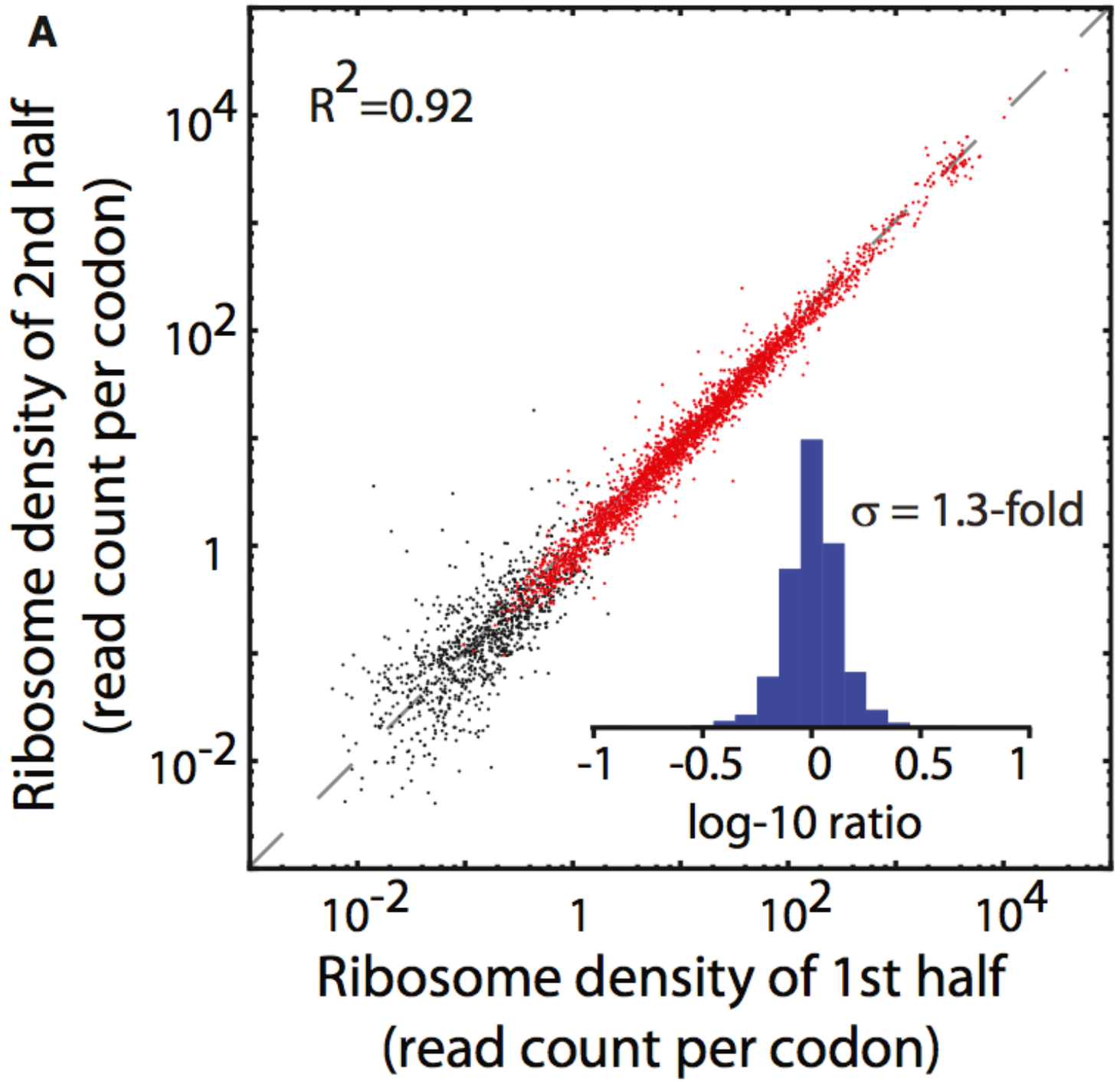

(A) Effect of translational pausing on average ribosome density. Average ribosome density is plotted for the first and second half of each gene. The Pearson correlation for genes with at least 64 reads aligned to both halves (red) is $R^2 = 0.92$. The inset shows the distribution of the fold difference between the second and the first halves (n = 2,870; SD, 1.3-fold).

Figure S1 Adjustment to Ribosome Density Based on Sequence and Position Specific Variation in Translation Elongation Rates, Related to Fig.1A

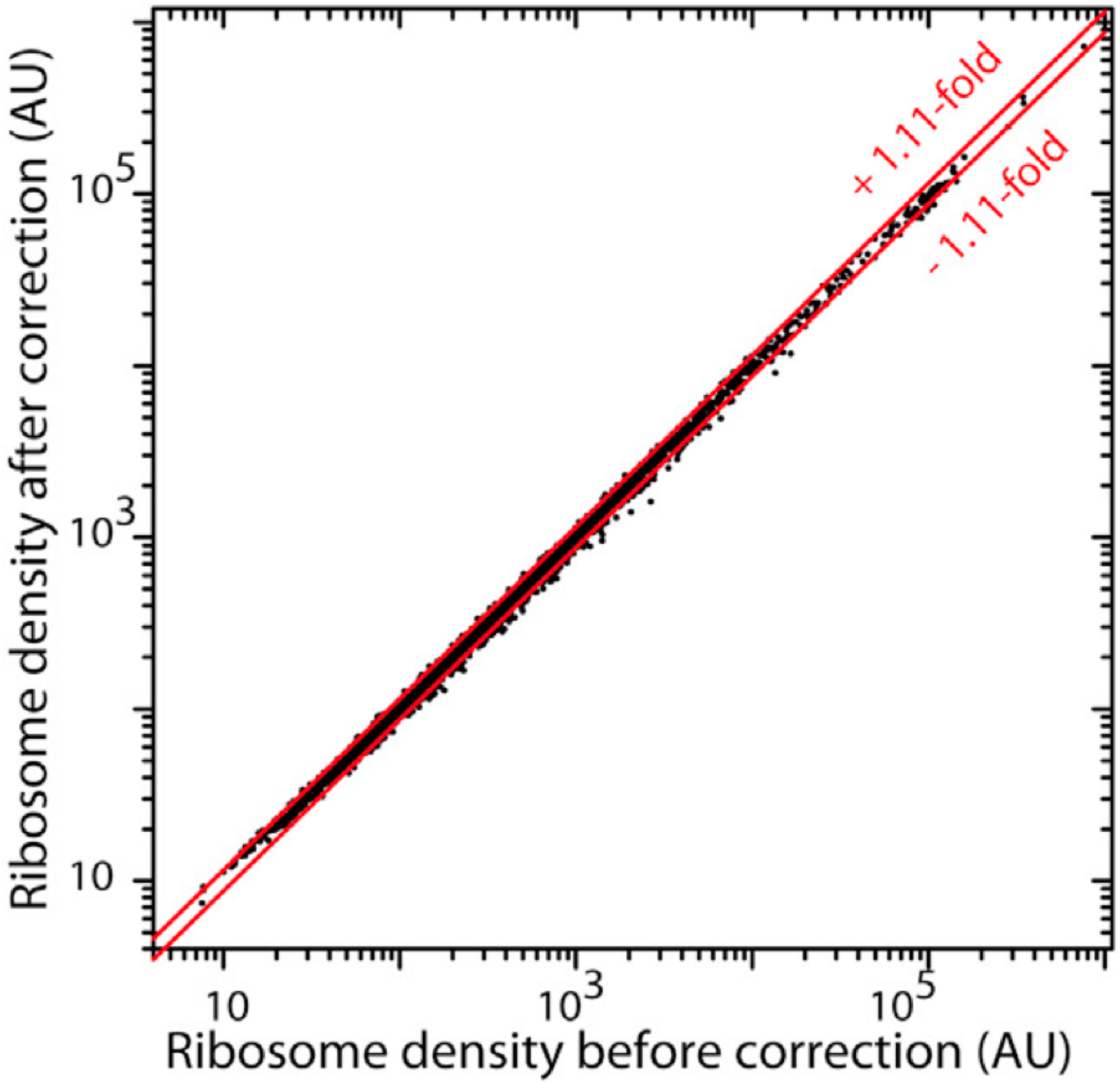

(D) Effects of the corrections for local variation in translation elongation rates. For each gene, the average ribosome density before and after corrections is plotted. The standard deviation for the differences is 1.11-fold.

Figure1

Absolute Quantification of Protein Synthesis Rates

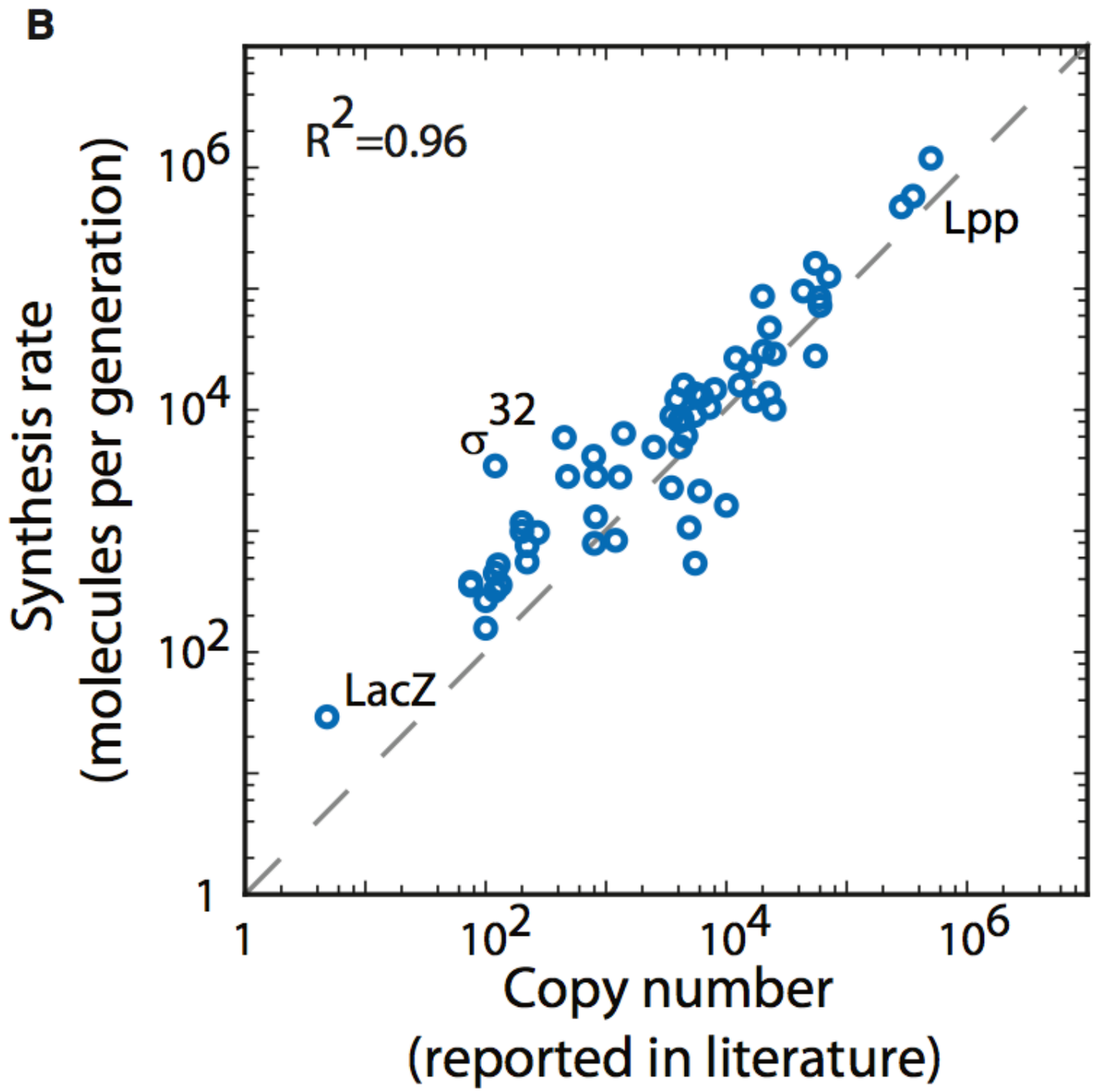

(B) Agreement between published protein copy numbers and absolute synthesis rates. The copy numbers of 62 proteins that have been individually quantified in the literature are plotted against the absolute protein synthesis rates (Pearson correlation, $R^2 = 0.96$).

Figure S2 Comparison of Published Quantitative Proteomics Measurements and Individually Measured Protein Copy Number, Related to Figure 1B

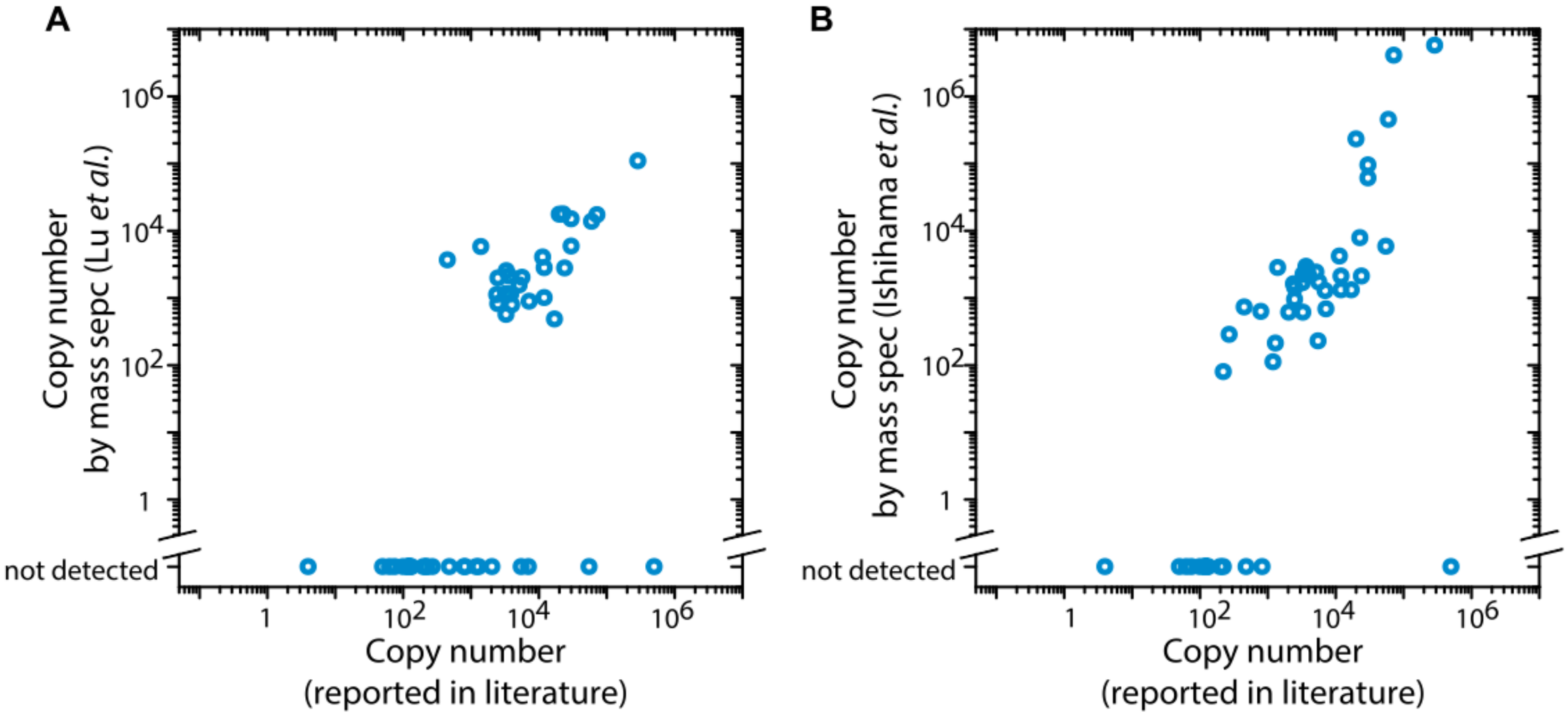

(A) Proteomics data using absolute protein expression (APEX) profiling based on mass spectrometry (Lu et al., 2007).
(B) Proteomics data using exponentially modifies protein abundance index (emPAI) based on mass spectrometry (Ishihama et al., 2008).

Figure S2 Comparison of Published Quantitative Proteomics Measurements and Individually Measured Protein Copy Number, Related to Figure 1B

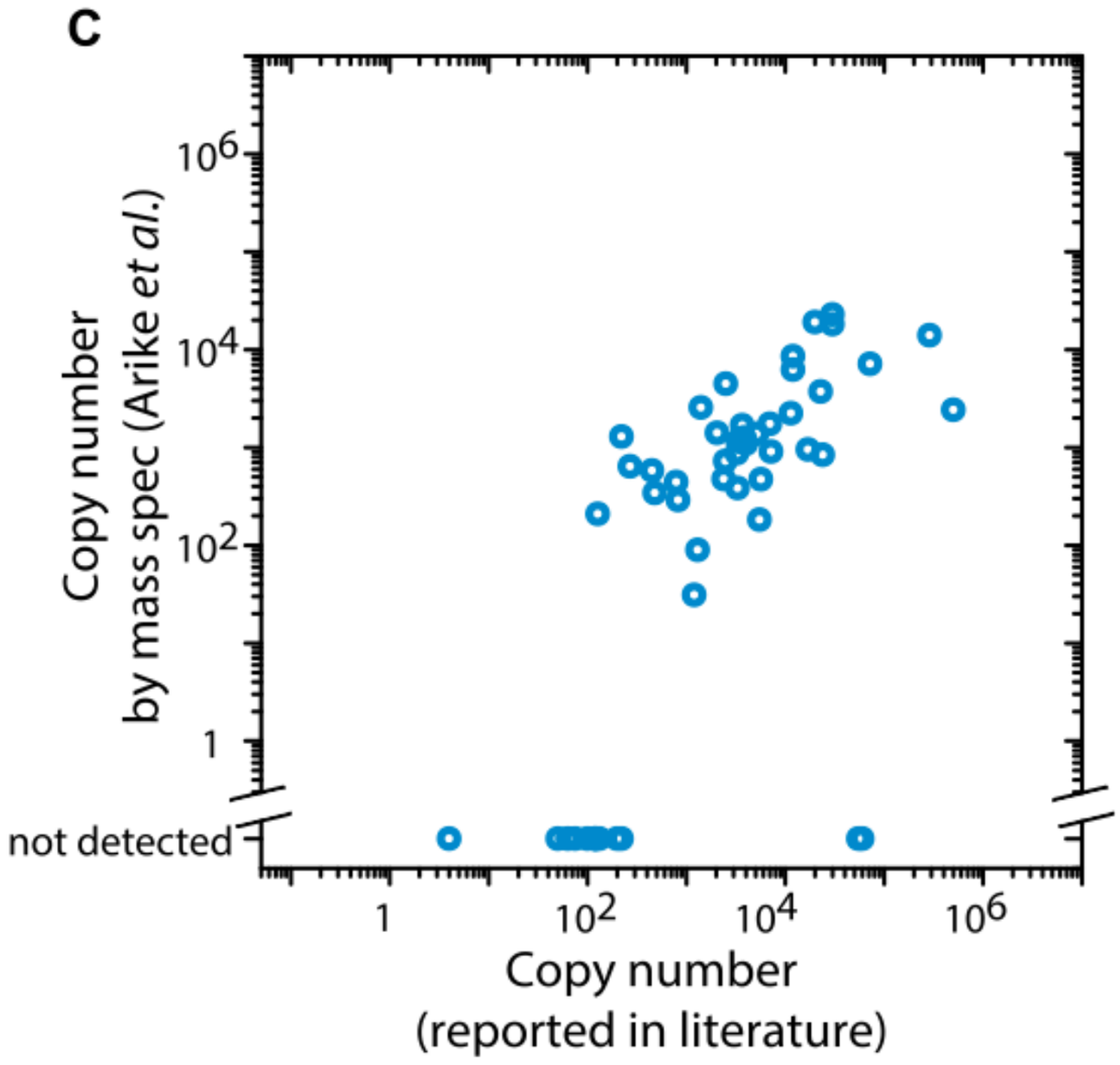

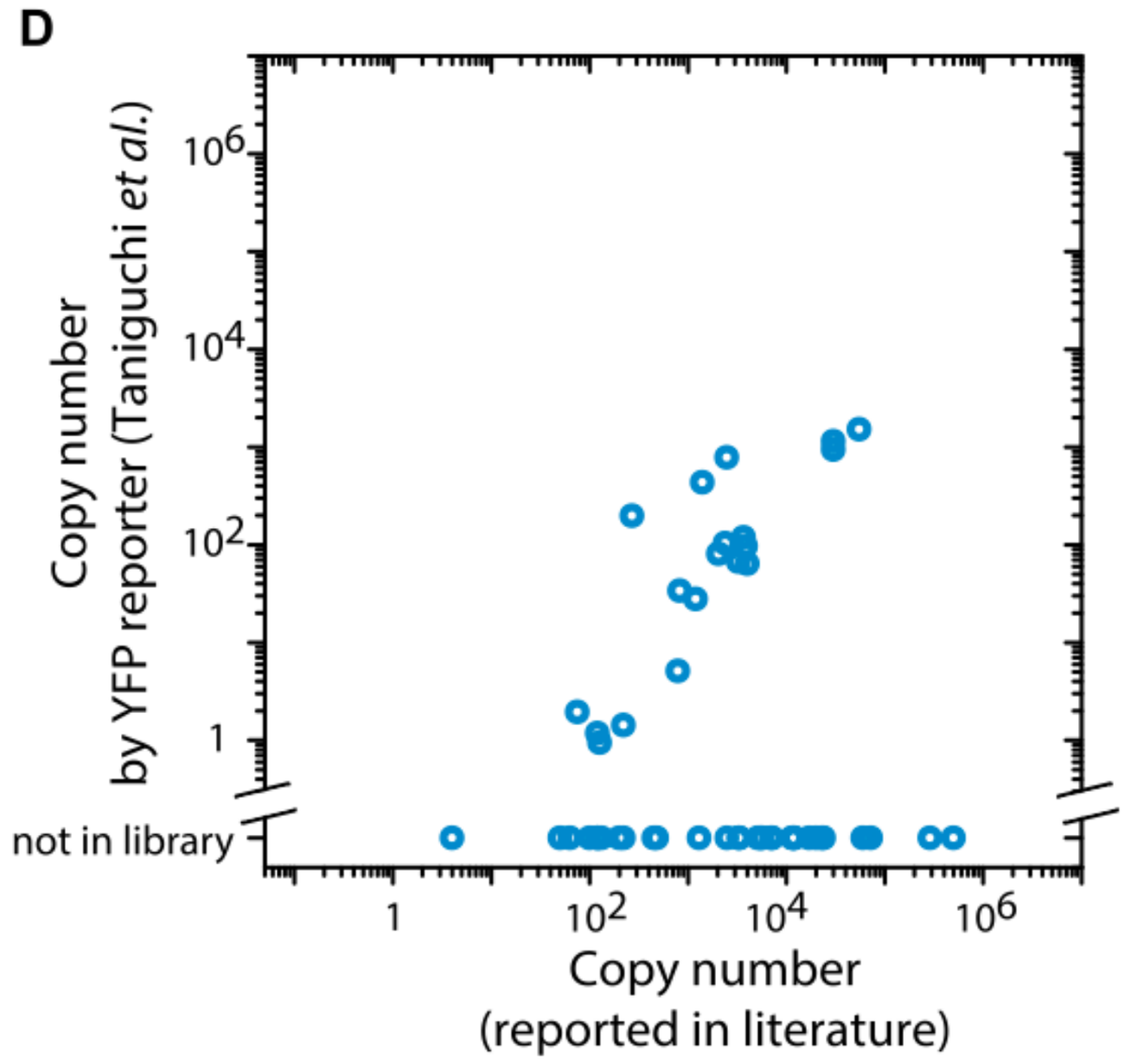

(C) Proteomics data using intensity-based absolute quantification (iBAQ) based on mass spectrometry (Arike et al., 2012). We note that the data in (A)–(C) were obtained using label-free quantification. Current development in other absolute quantification methods using isotopic labeling and synthetic peptides as standards could provide improvements in accuracy and coverage (Hanke et al., 2008; Picotti et al., 2009).

(D) Proteomics data using a YFP-fusion library (Taniguchi et al., 2010). The library was constructed for ~25% of the genome. The measurements were performed at a lower growth rate (150 min per doubling) compared to other reports, which gave rise to lower protein abundance in general.

Proportional Synthesis of Multi-protein Complexes.

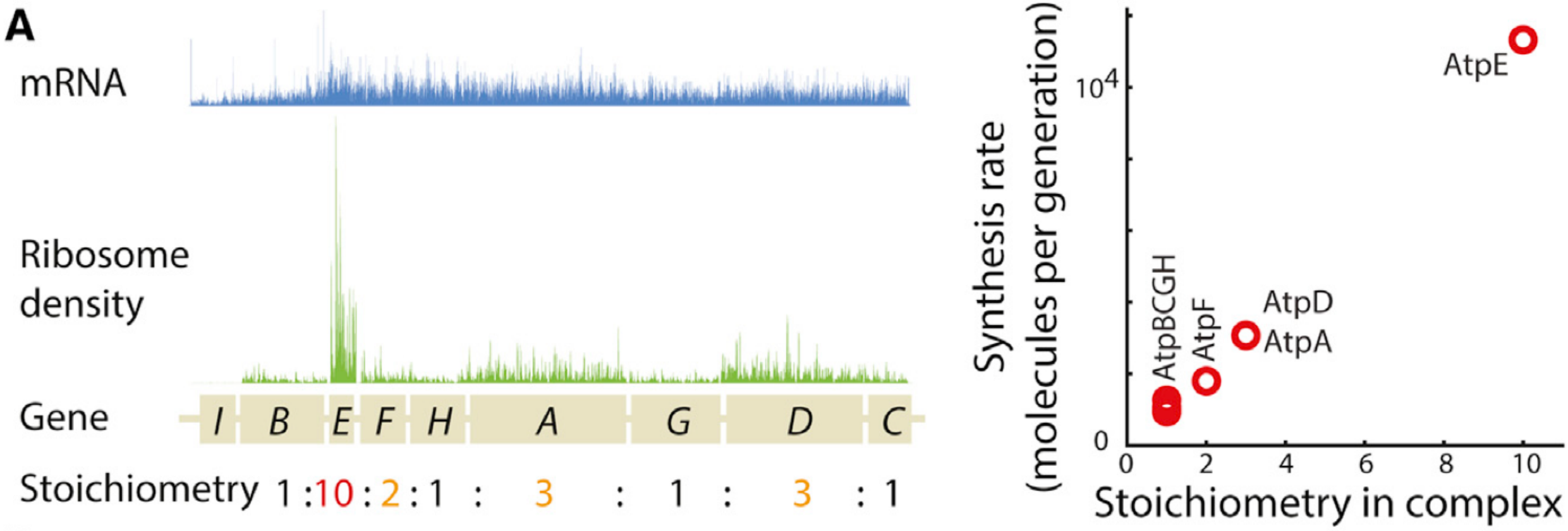

(A) Translation rates reflecting subunit stoichiometry for the ATP operon. Eight subunits of the F_0F_1 ATP synthase are expressed from a polycistronic mRNA, whose level as measured by RNA-seq is shown in blue. Each subunit is associated with different levels of ribosome density (green), and the average density is proportional to the subunit stoichiometry (right).

Proportional Synthesis of Multi-protein Complexes.

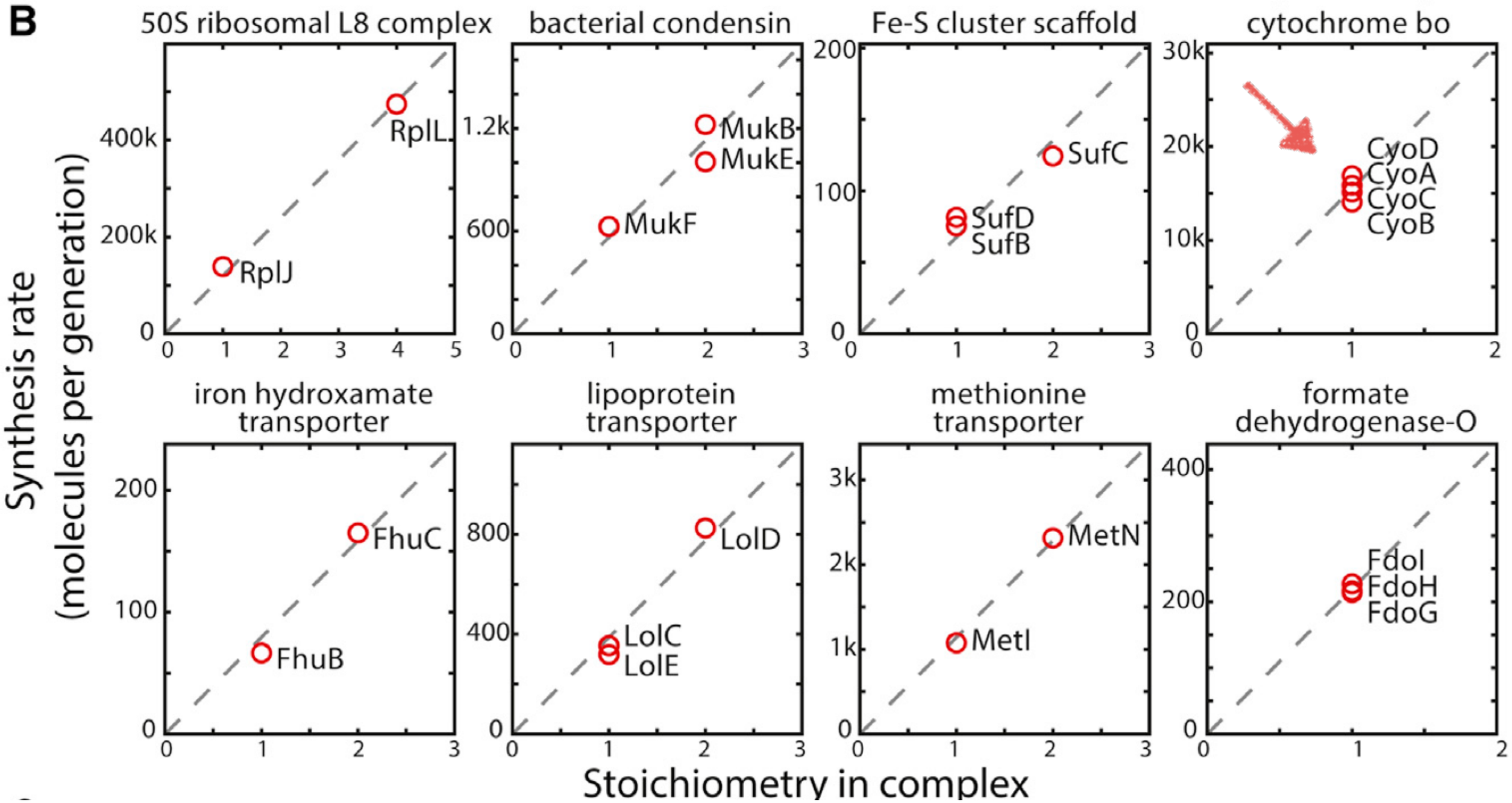

(B) Proportional synthesis for a diverse range of complexes. Synthesis rates are plotted as a function of the subunit stoichiometry for multi-protein complexes whose subunits are encoded in the same operon. Complexes with different subunit stoichiometry or more than two subunits are included here (also see C). The dashed line indicates the best fit that crosses the origin.

Figure S4 Proportional Synthesis at 10C, mRNA Levels, and Gene Order, Related to Figure 2

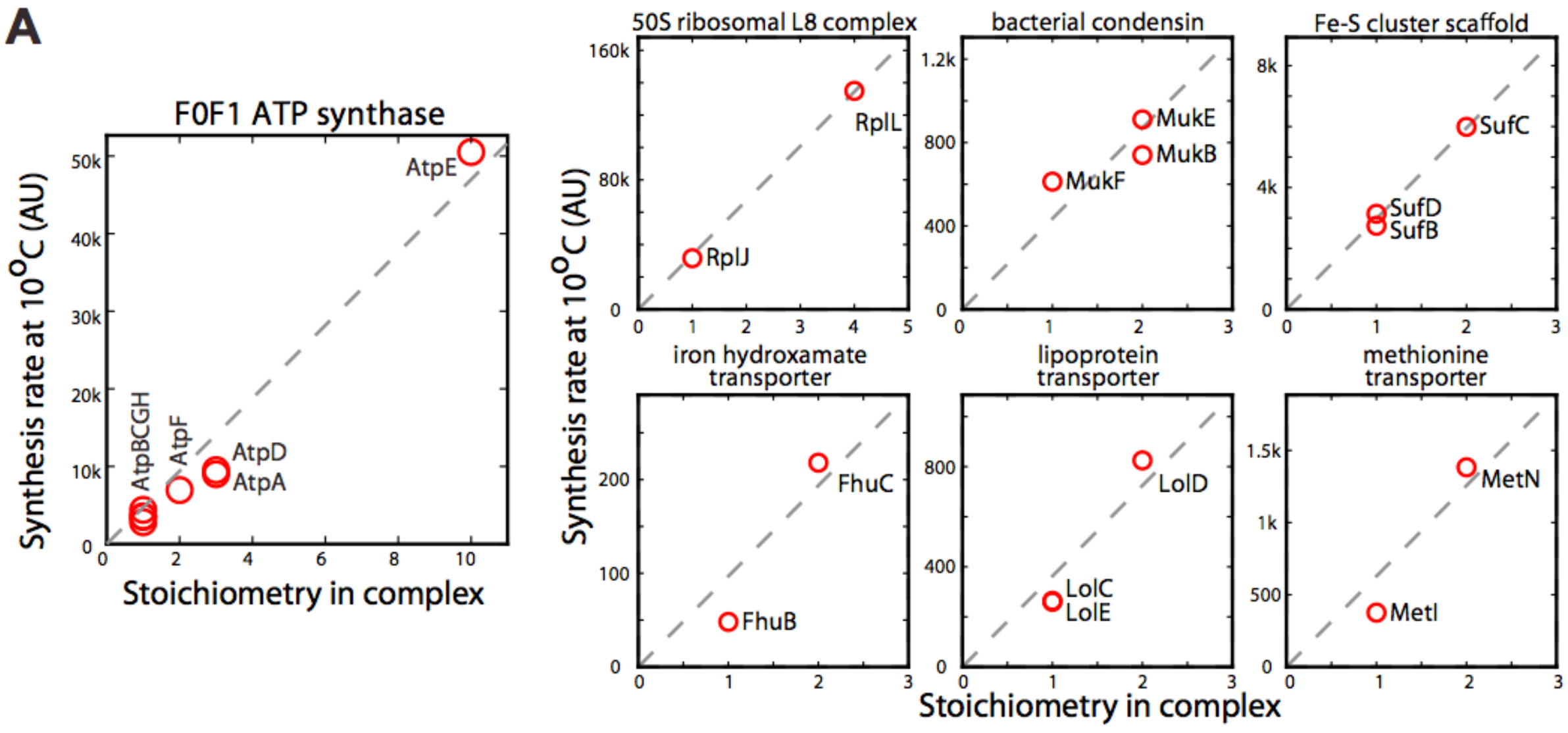

(A) Proportional synthesis at 10°C. Synthesis rates relative to stoichiometry are plotted for complexes expressed from the same operon. Experiment was performed at 50 hr after shifting the culture to 10°C. The dashed line indicates the best-fit that crosses the origin.

Figure S3 Proportional Synthesis for Other Multiprotein Complexes, Related to Figure 2

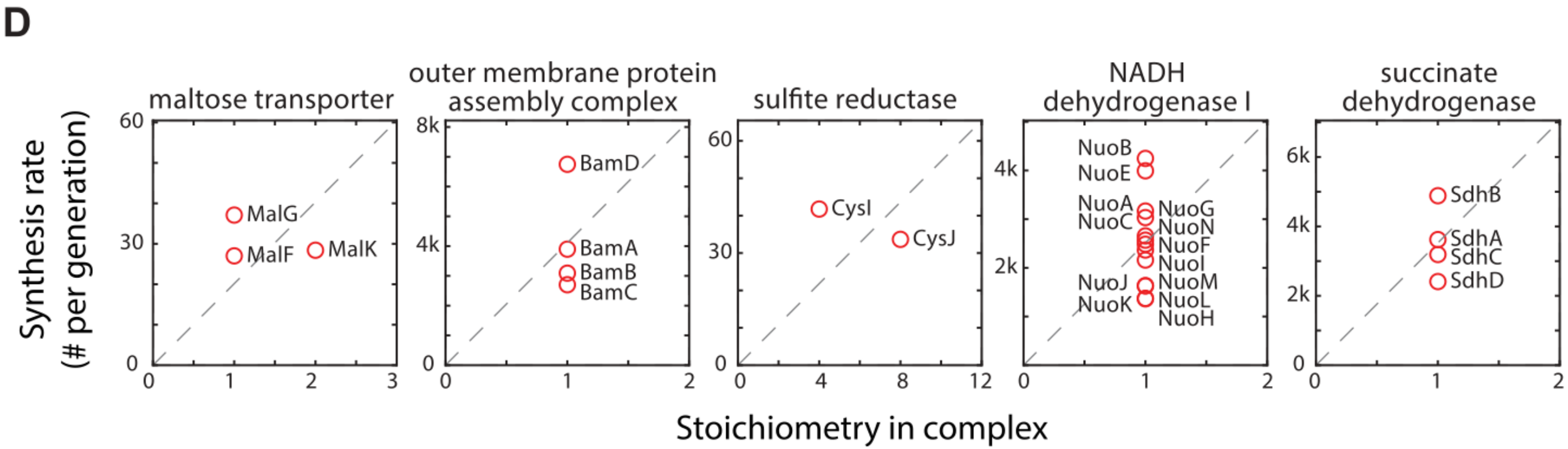

(D) Exceptions to proportional synthesis. Five complexes do not follow proportional synthesis out of 64 complexes. The synthesis rates relative to the stoichiometry are plotted here. Subunits of the maltose transporter and the BAM complex are translated from different mRNA, whereas the other three complexes are translated from the same polycistronic mRNA.

Proportional Synthesis of Multi-protein Complexes.

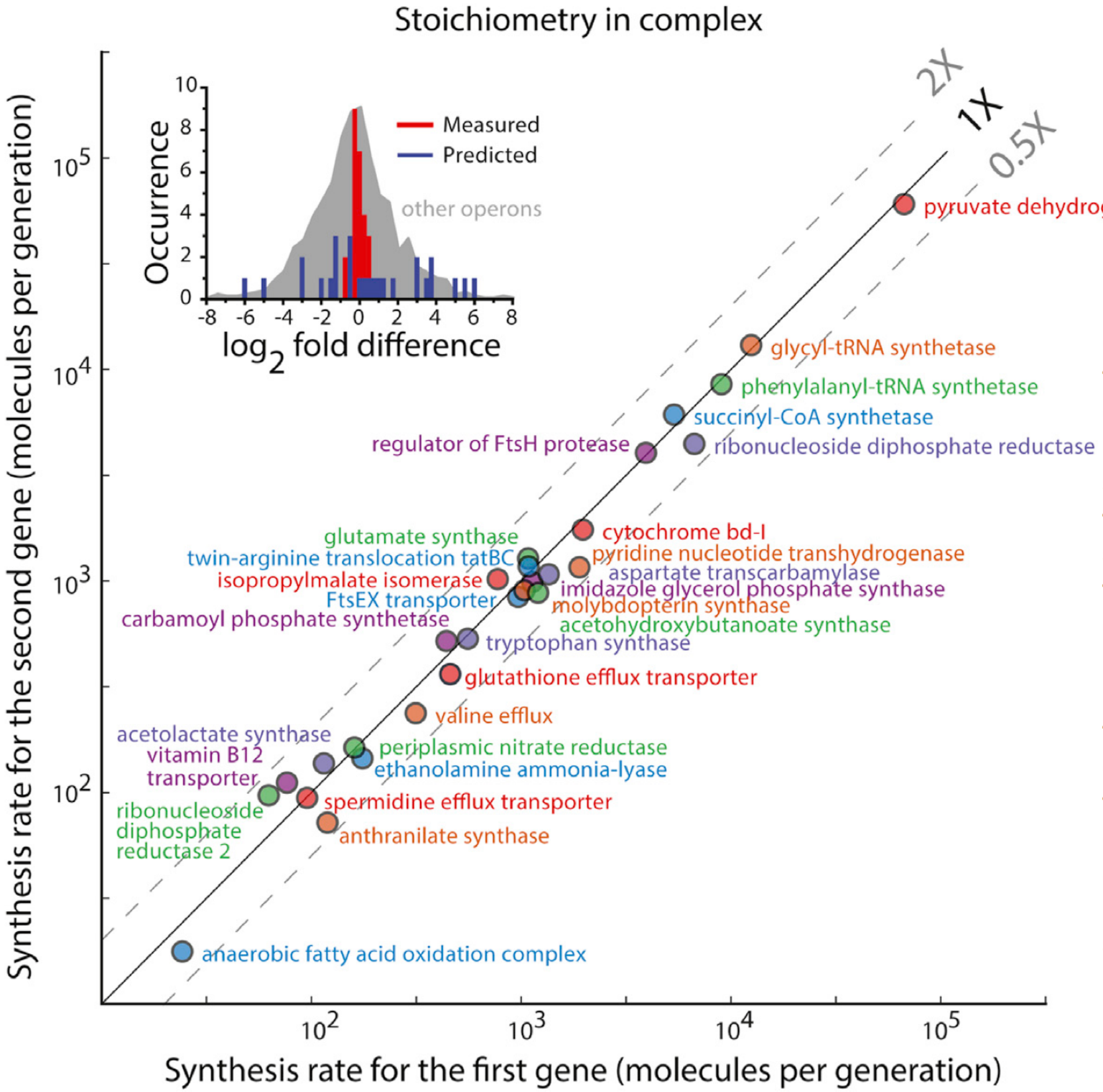

(C) Proportional synthesis for complexes with two equimolar subunits. Each complex is plotted for the synthesis rates of the two subunits, with the earlier (later) gene in the operon on the horizontal (vertical) axis. A total of 28 equimolar and cotranscribed complexes, covering 4 orders of magnitude in expression level, are plotted here. Inset shows the histogram of fold difference between the synthesis rates of the two subunits. Our experimental results are shown in red, and the predicted values based on a thermodynamic model considering the sequence surrounding translation initiation sites are shown in blue (Salis et al., 2009). The distribution of the differences in translation rates for all other operons is shown in gray. (B) and (C) show complexes whose subunits are encoded on a single polycistronic operon. See Figures S3B and S3C for examples of proportional synthesis involving distinct transcripts.

Figure S3 Proportional Synthesis for Other Multiprotein Complexes, Related to Figure 2

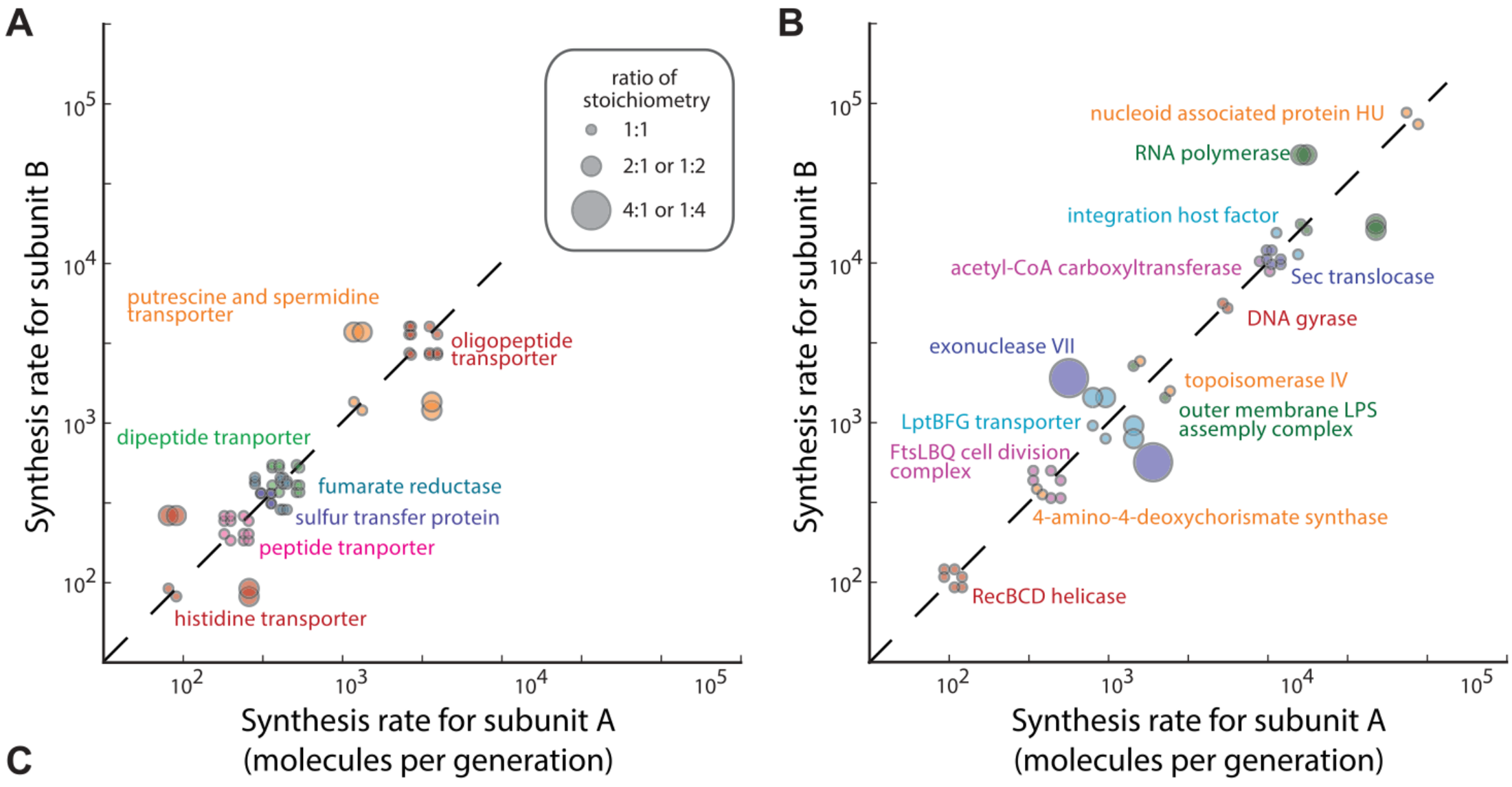

(A) Proportional synthesis for complexes whose members are encoded in the same operon. Complexes not included in Figure 2B are shown here. The synthesis rate for each pair of subunits in the complex is plotted, with the identity of the complex indicated by the color code. The size of the symbol reflects the ratio of stoichiometry between the pair. Each pair is plotted twice with different order.

(B) Proportional synthesis for complexes whose members are encoded in more than one operon. The size of symbols is the same as in (A). Inset shows synthesis rates for ribosomal proteins. For some of the ribosomal protein with equal stoichiometry, proportional synthesis may be achieved by a combination of translational coupling and auto-regulation.

Figure S3 Proportional Synthesis for Other Multiprotein Complexes, Related to Figure 2

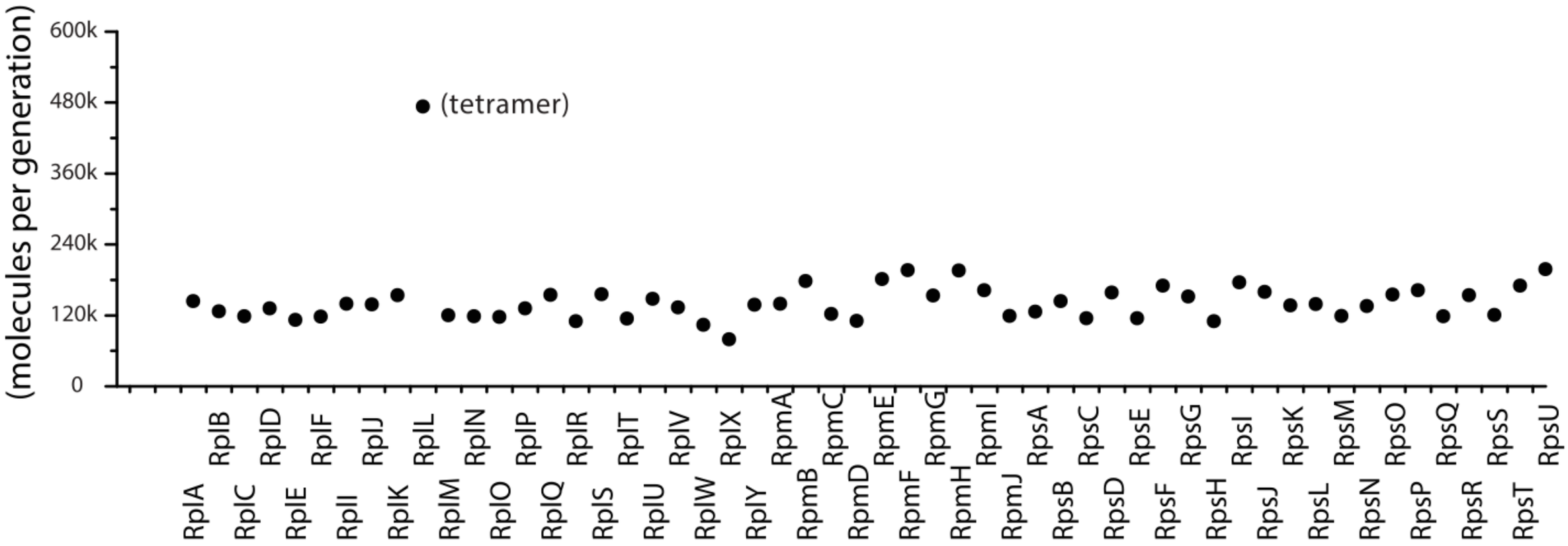

(C) Proportional synthesis for ribosomal proteins. All proteins, except RplL (L7/L12), have the stoichiometry of one per ribosome.

Proportional Synthesis for Complexes in Yeast.

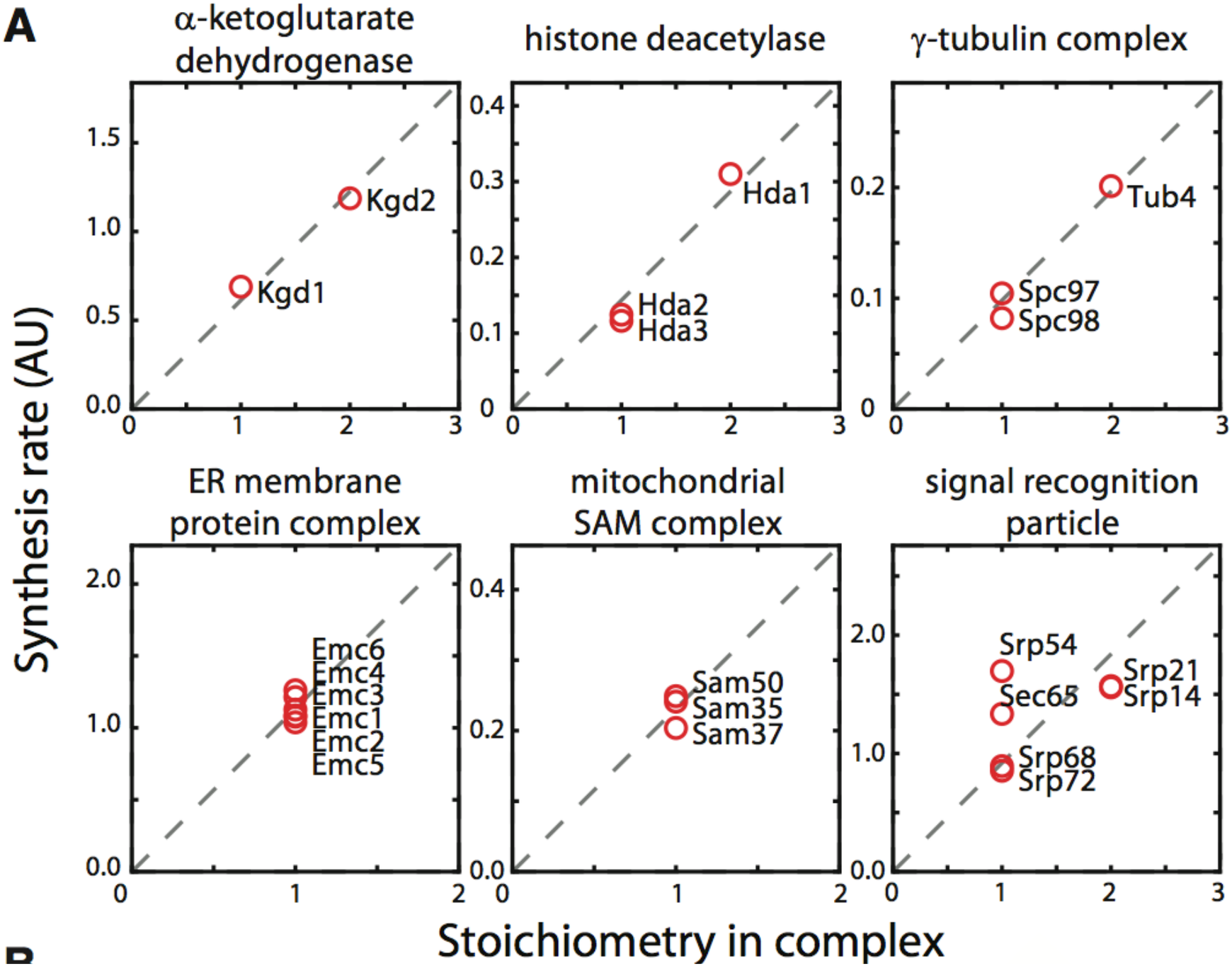

(A) Proportional synthesis for multiprotein complexes in *S. cerevisiae*. Synthesis rates are plotted as a function of the subunit stoichiometry for complexes with more than two subunits. For the signal recognition particle, four subunits (Srp14/Srp21/Srp68/Srp72) are synthesized according to their stoichiometry, and the other two are exceptions.

Proportional Synthesis for Complexes in Yeast.

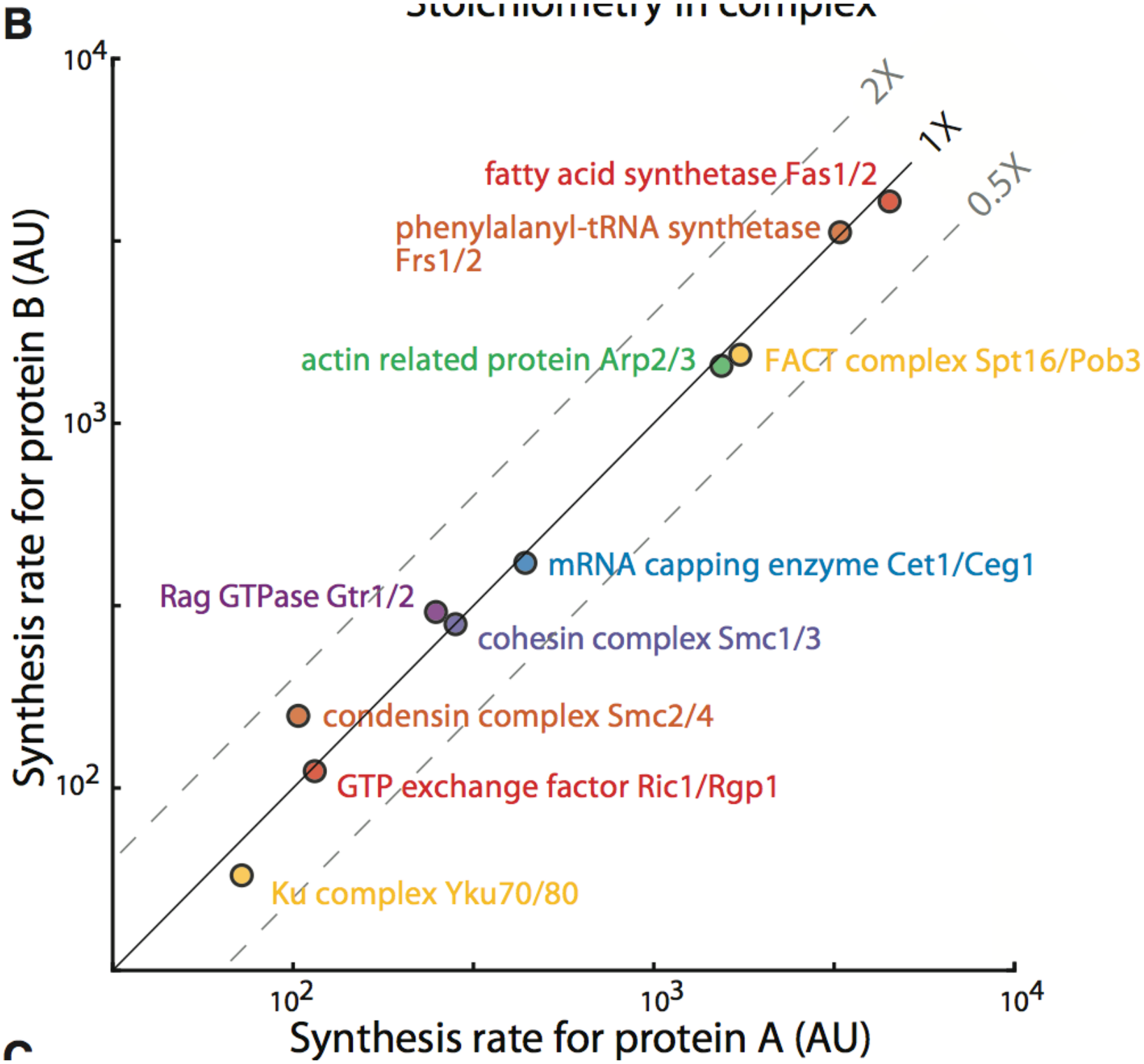

(B) Proportional synthesis for heterodimeric complexes in *S. cerevisiae*. Each complex is plotted for the synthesis rate of the two subunits.

Proportional Synthesis for Complexes in Yeast.

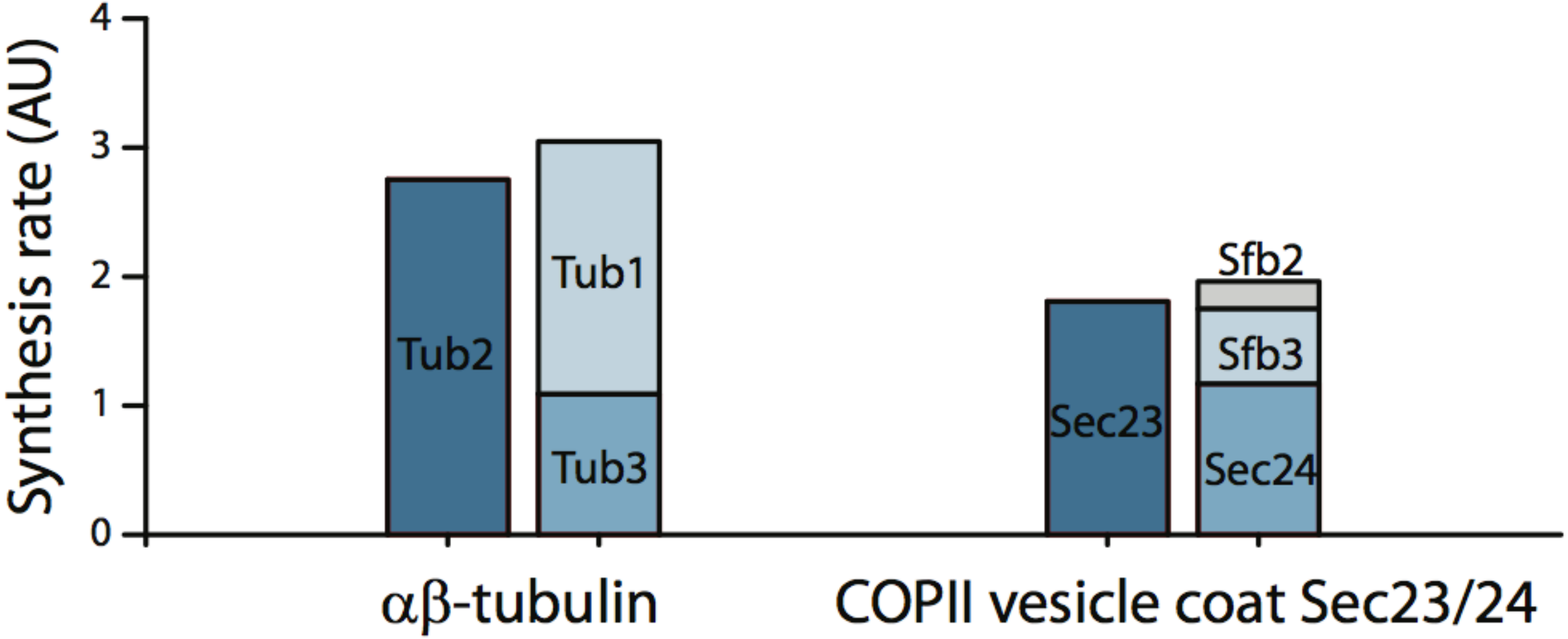

(C) Proportional synthesis for complexes with paralogous subunits. For each complex, the subunits that can substitute each other are plotted in the same column.

Hierarchical expression for Functional Models

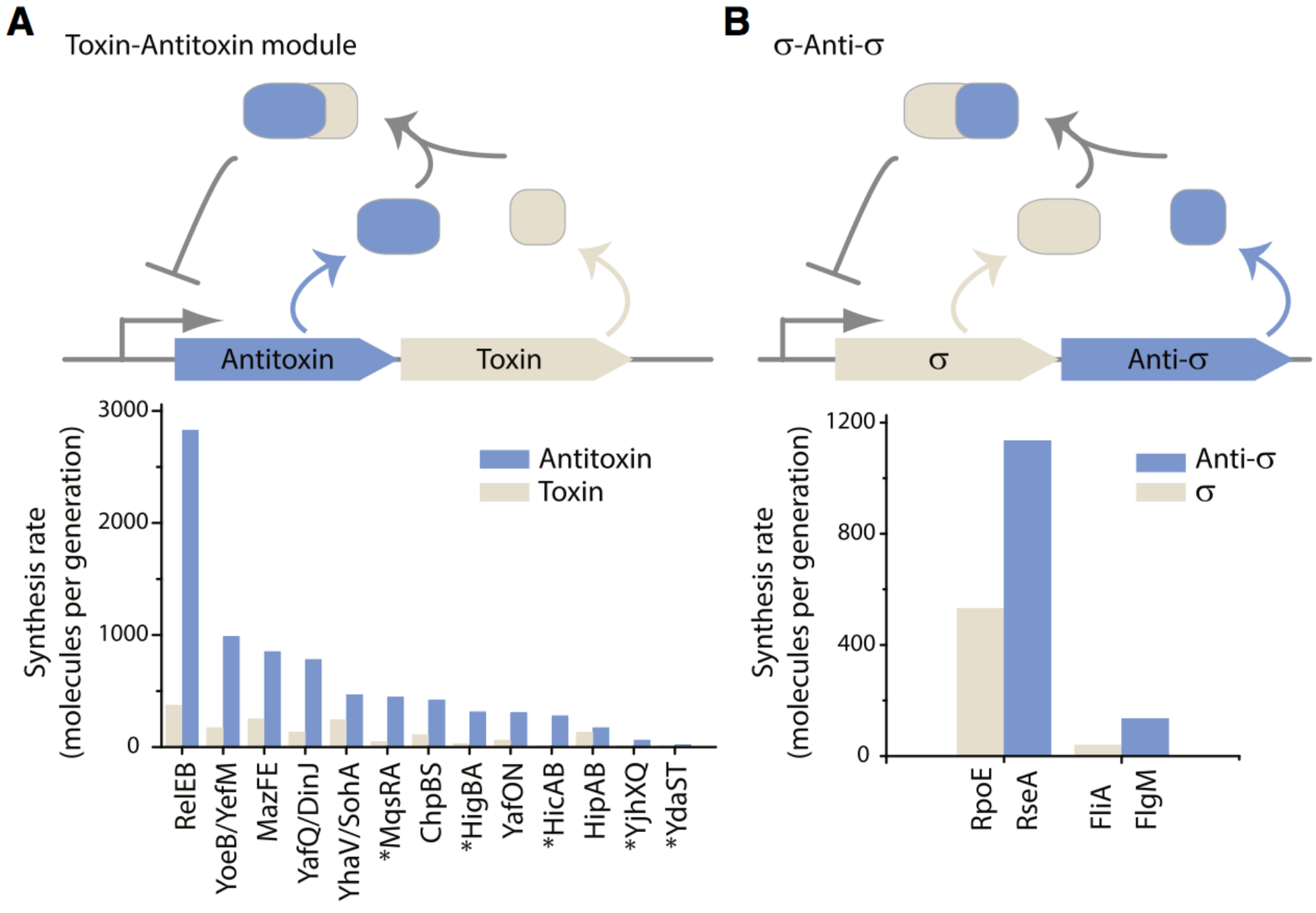

(A) Synthesis rates for TA modules. *E. coli* contains 12 type II TA systems that are each expressed from a polycistronic mRNA. (The order of genes differs among systems.) The antitoxin protein binds to and inhibits the toxin protein, while re-pressing its own transcription. The synthesis rates for each system are plotted (bottom). Modules with the toxin gene preceding the antitoxin gene in the operon are marked by an asterisk.

(B) Synthesis rates for σ-anti-σ modules. The anti-σ binds to and inhibits the σ, preventing transcription from the promoter driven by the corresponding σ. The synthesis rates for each system are plotted (bottom).

Hierarchical expression for Functional Models

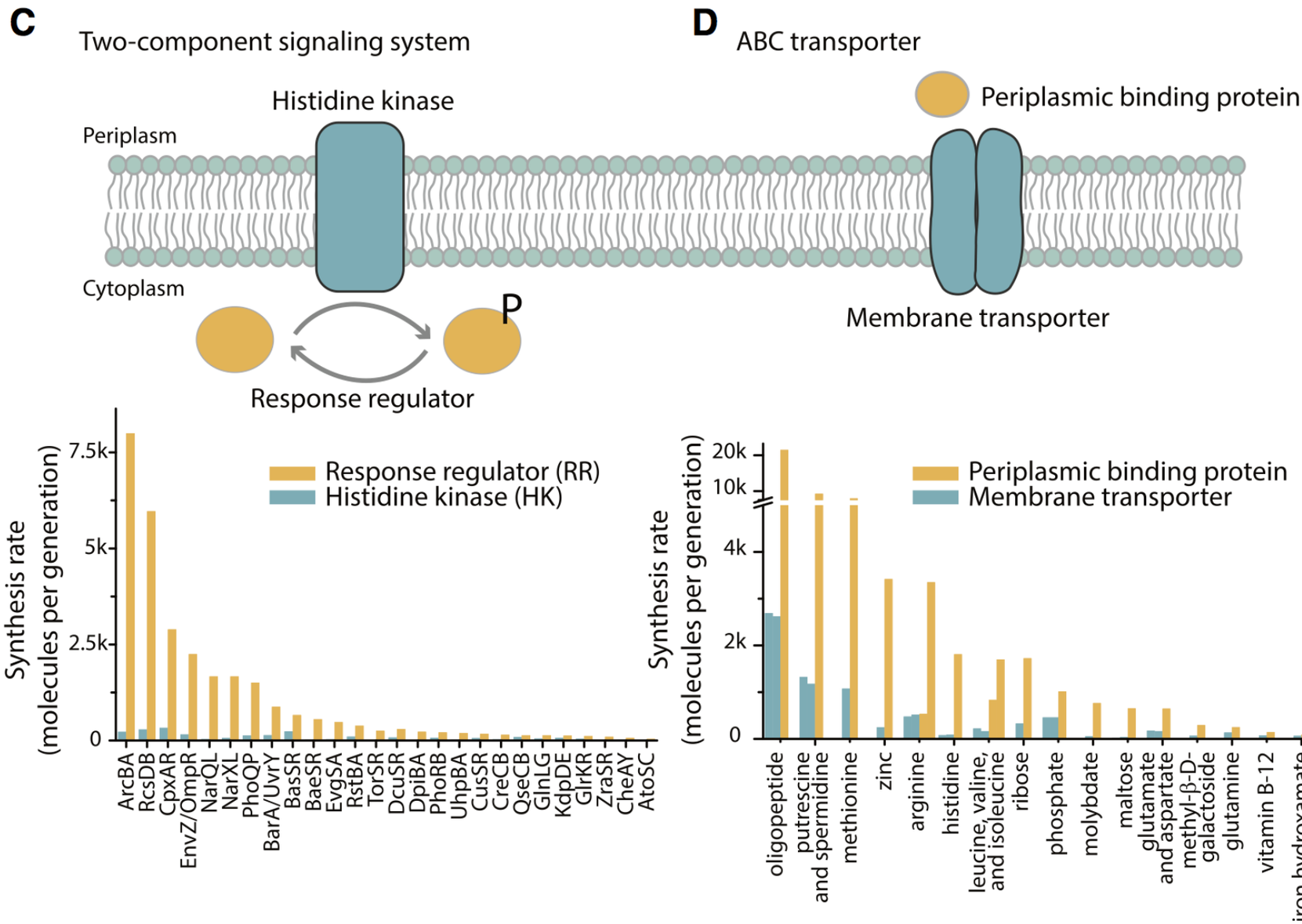

(C) Synthesis rates for two-component signaling systems. Bacterial two-component signaling system consists of a membrane-bound HK and the cognate RR. The synthesis rates for 26 two-component systems in *E. coli* are plotted (bottom).

(D) Synthesis rates for ABC transporters. An ABC transporter consists of a core membrane transporter, an ATP-binding domain, and the corresponding periplasmic-binding proteins. The synthesis rates for each transporter are plotted (bottom).

Composition of the E. coli Proteome

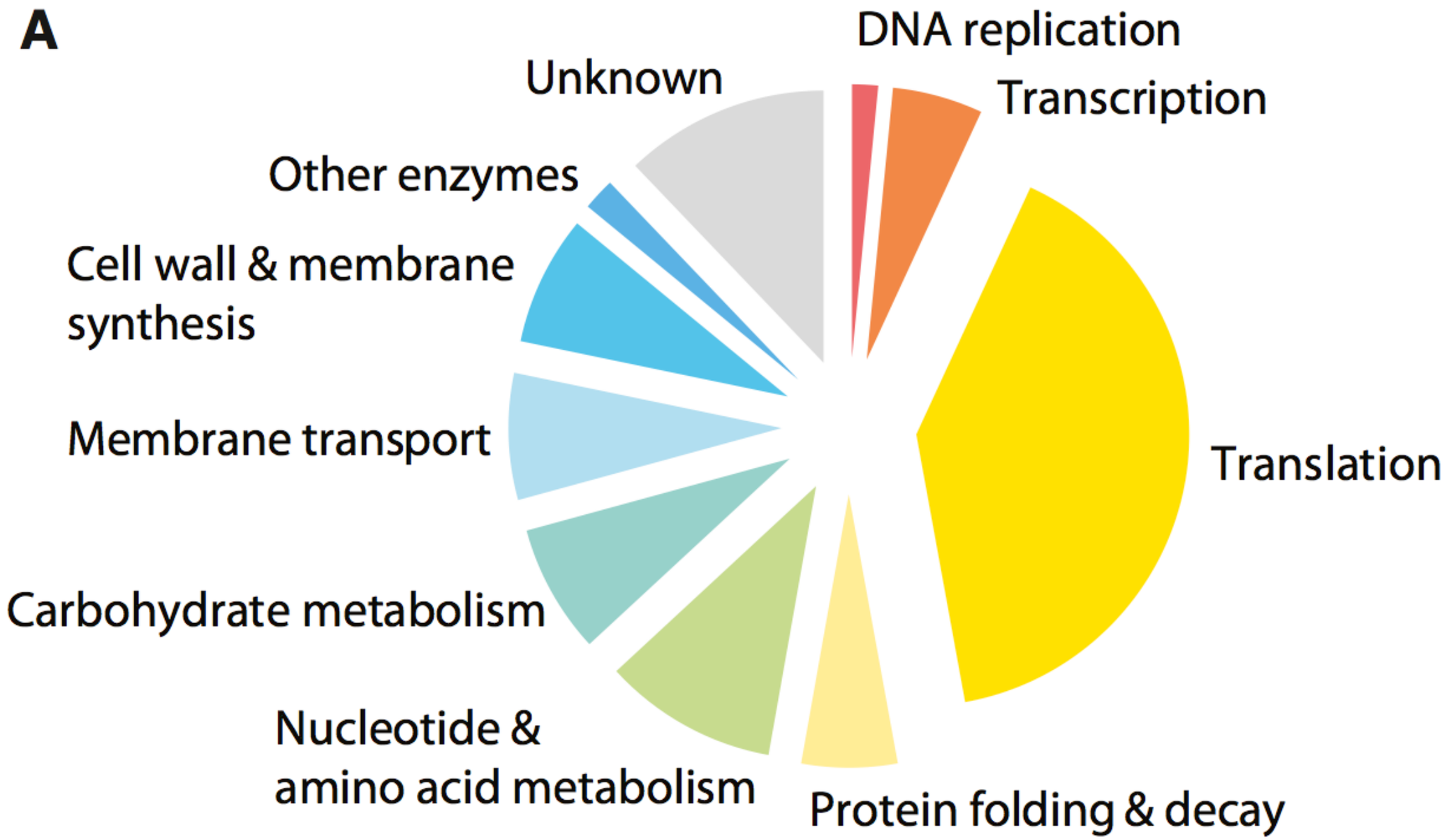

(A) Breakdown of the proteome by functions. The mass fraction of the proteome that is devoted to specific biological functions is plotted as a pie chart. The copy numbers were estimated for *E. coli* grown in rich defined medium

Composition of the E. coli Proteome

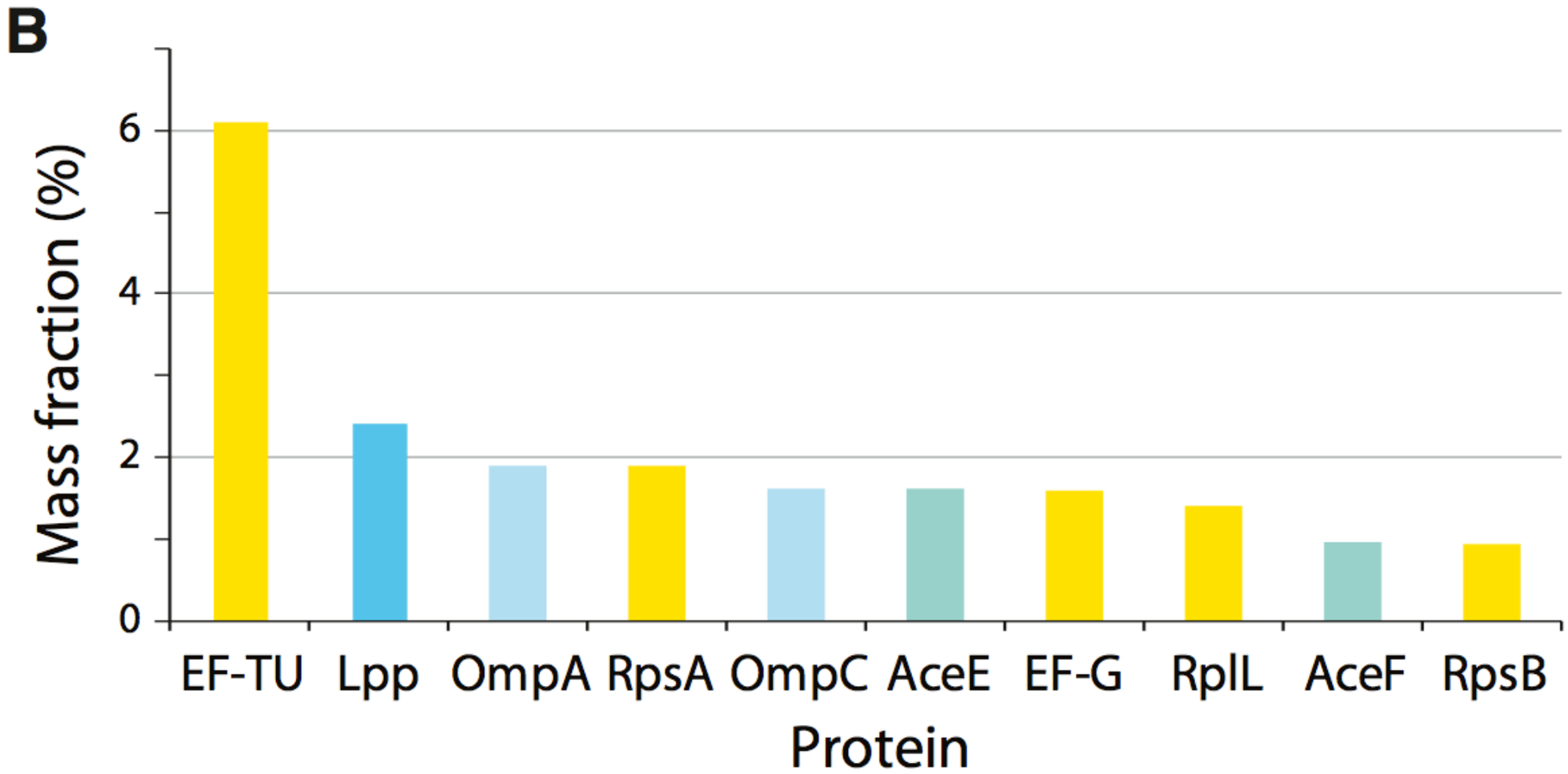

(B) Ten proteins with the largest mass fraction in the proteome. The color used for each protein corresponds to the biological function indicated in (A).

Abundance of TF.

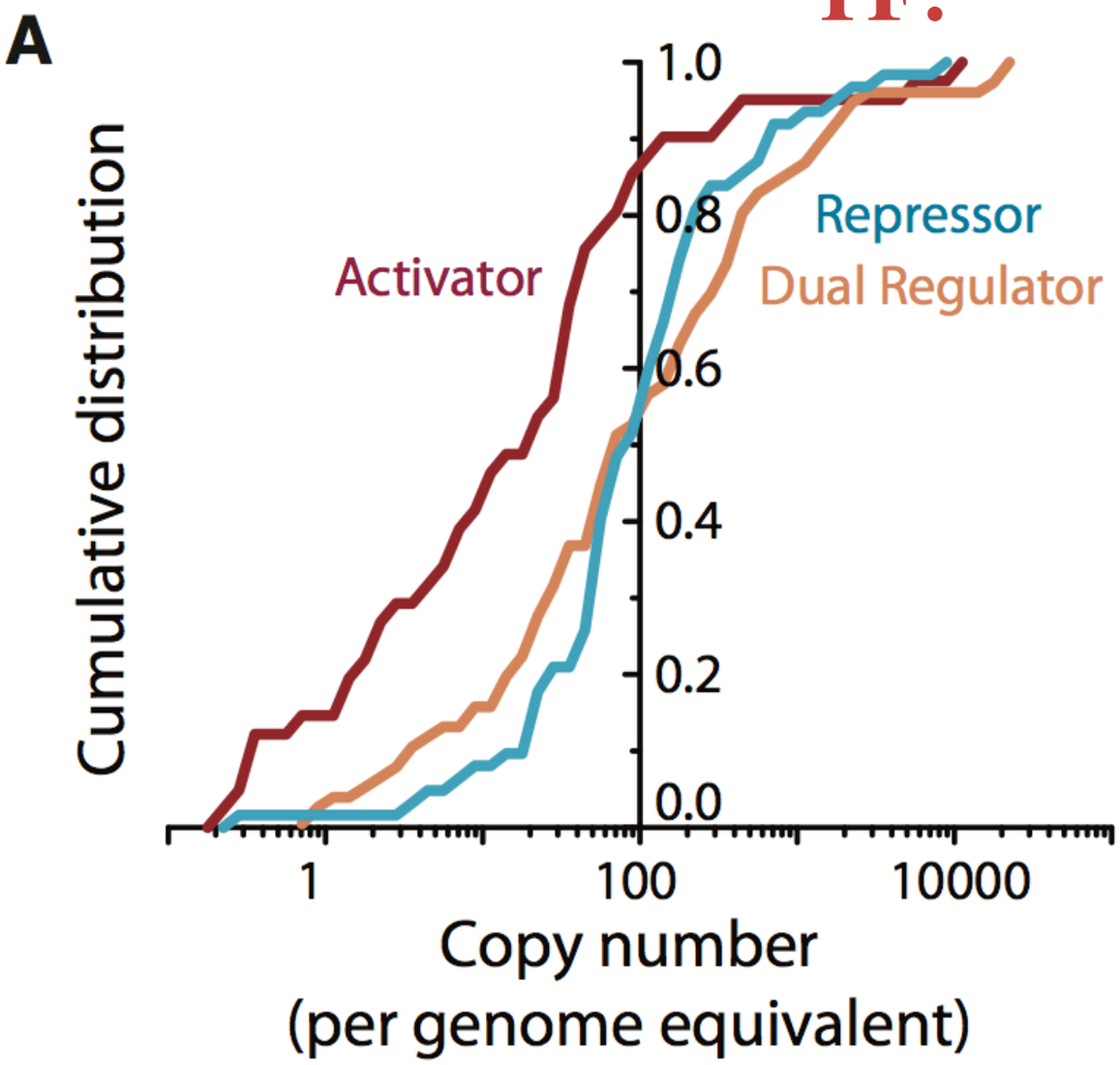

(A) Cumulative distribution of abundance for transcriptional activators, repressors, and dual regulators. The cumulative distribution for each class of TF is plotted as a function of the copy number per genome equivalent.

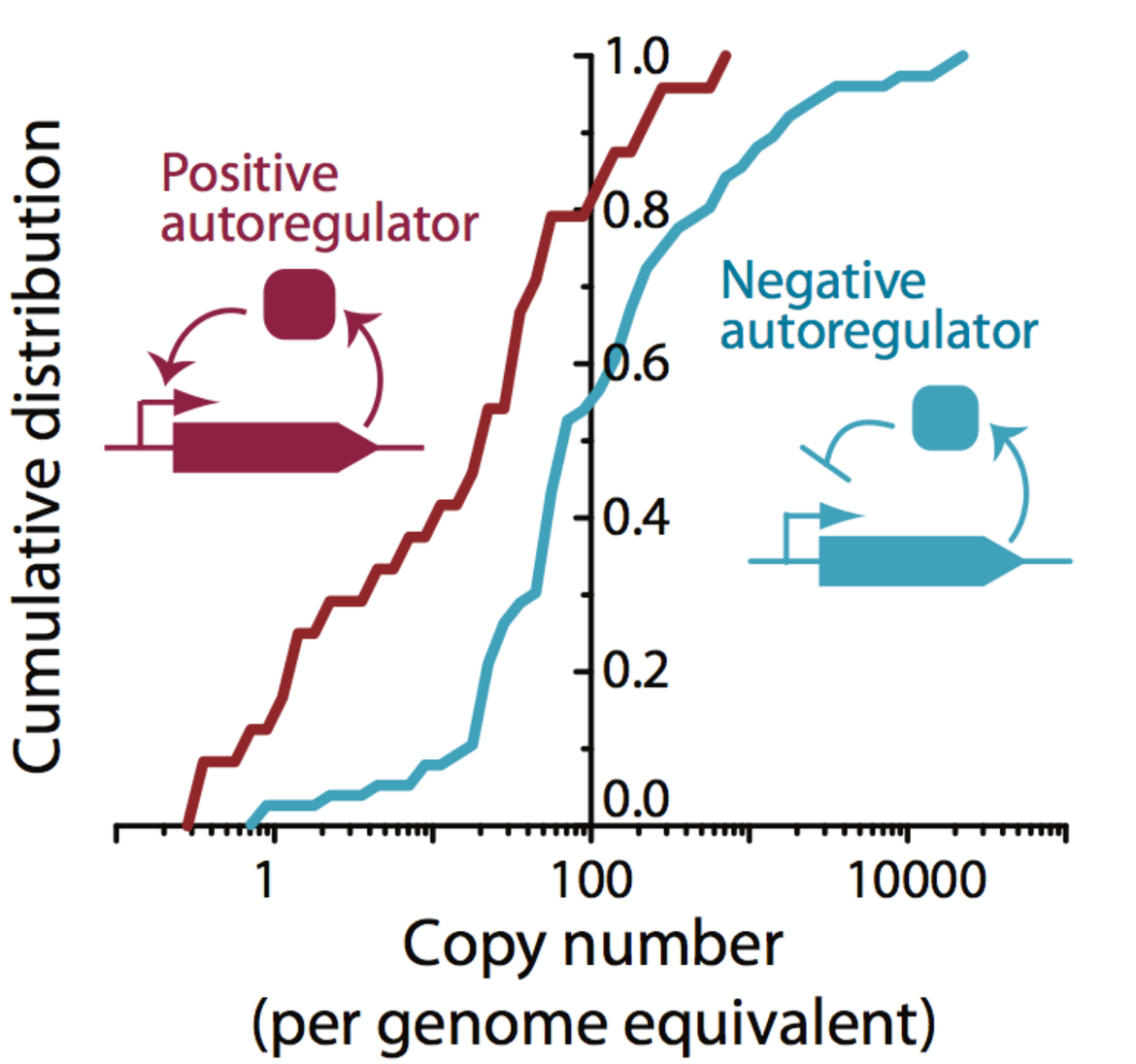

(B) Cumulative distribution of abundance for autoregulators. The cumulative distributions for positive and negative autoregulators are plotted as a function of the copy number per genome equivalent.

Abundance of TF.

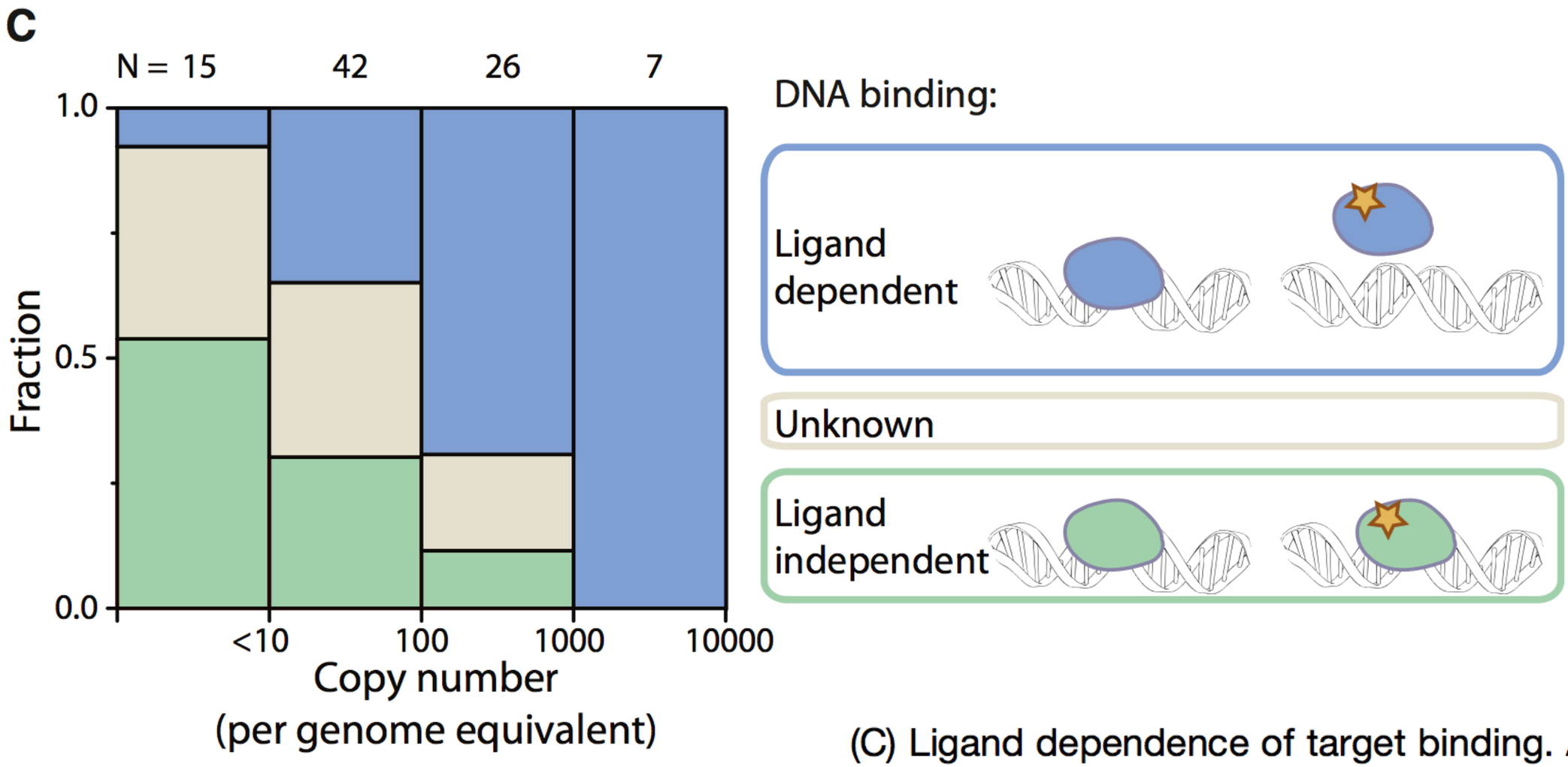

(C) Ligand dependence of target binding. Among TFs whose abundance falls into a given range, the fraction that binds to the target site in a ligand-dependent way is shown in blue, and the fraction that binds to the target site independent of ligands is shown in green. The number of TFs analyzed is indicated above each bin.

Quantitative Analysis of the Met Biosynthesis Pathway

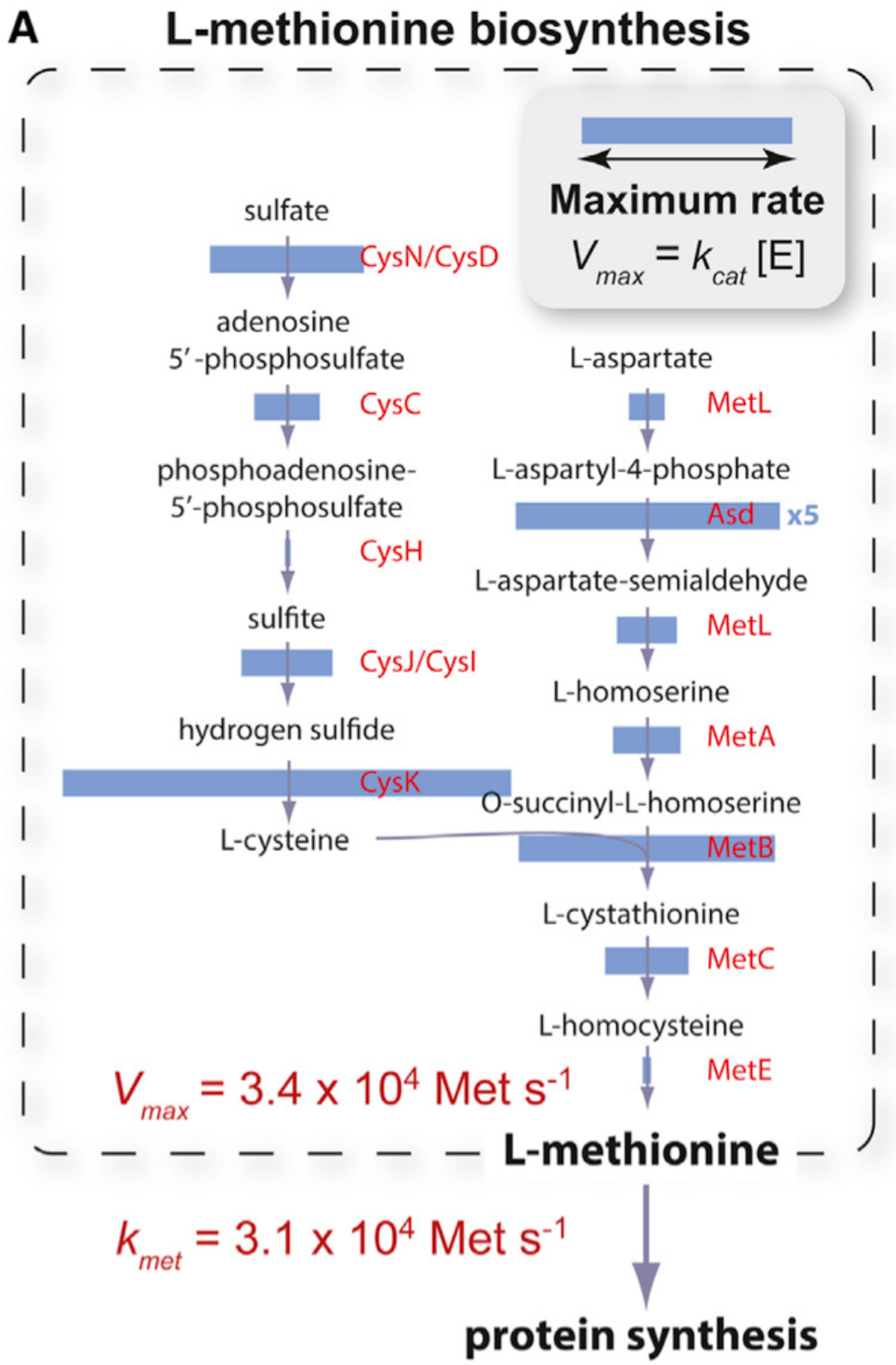

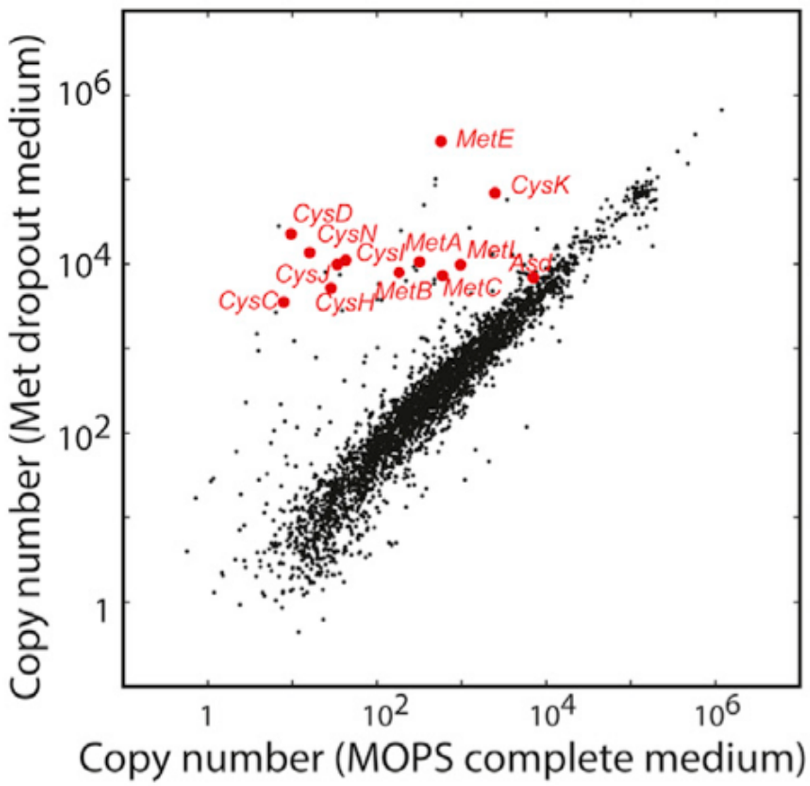

(A) Maximal reaction rates for the intermediate steps. For each step of the pathway, the V_{max}, inferred from the enzyme abundance in vivo and the k_{cat} measured in vitro, is shown as the width of the blue bar. The last step that is catalyzed by the enzyme MetE has a V_{max} of 34,000 Met/s/cell, whereas the flux of Met into protein synthesis is 31,000 Met/s/cell. The scatterplot on the right shows upregulation of these enzymes in media without Met. MOPS, 3-(N-morpholino)propane-sulfonic acid.

Quantitative Analysis of the Met Biosynthesis Pathway

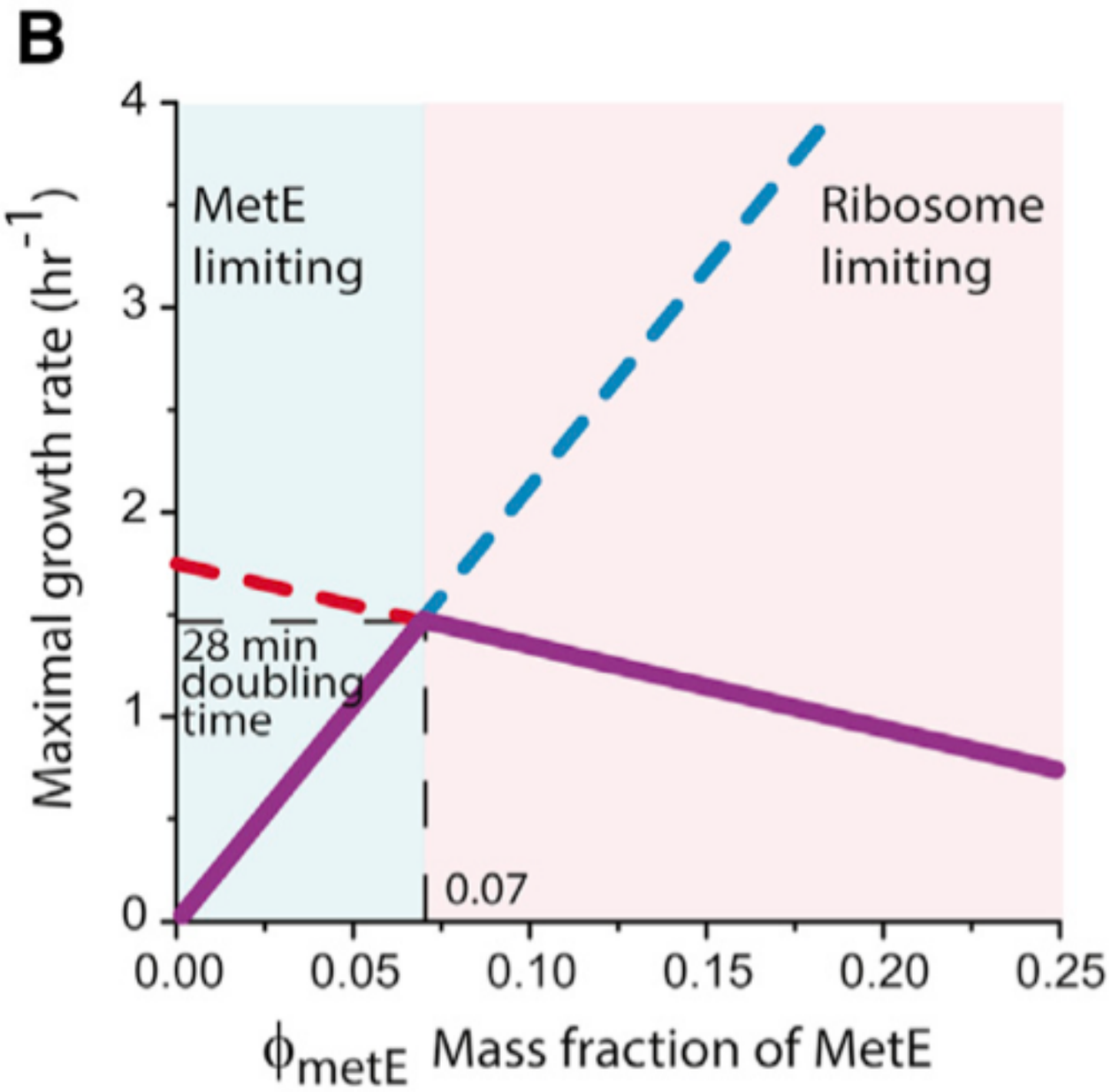

(B) Model predicting the optimal MetE level. In a model that considers the cost and benefit of MetE expression, the maximal growth rate is plotted as a function of the mass fraction of MetE in the proteome. The cost due to competition with new ribosome synthesis is shown in red, and the benefit from increased Met flux is shown in blue. The maximal growth rate is highest (28 min) when the mass fraction of MetE is ~7%. This prediction agrees with experimental results.

THANKS!